The Interplay of Aromaticity and Antiaromaticity in N-Doped Nanographenes

Isaac Benkyi, Olga Staszewska-Krajewska, Daniel T. Gryko,
Michal Jaszunski, Amnon Stanger, and Dage Sundholm

Just Accepted

1
2
3
4
5
6
7
8
9
10
11
12
13
14
15
16
17
18
19
20
21
22
23
24
25
26
27
28
29
30
31
32
33
34
35
36
37
38
39
40
41
42
43
44
45
46
47
48
49
50
51
52
53
54
55
56
57
58
59
60

The Interplay of Aromaticity and Antiaromaticity in N-Doped Nanographenes

Isaac Benkyi,[†] Olga Staszewska-Krajewska,[‡] Daniel T. Gryko,[‡]

Michał Jaszuński,*,[‡] Amnon Stanger,*,[¶] and Dage Sundholm*,[§]

University of Helsinki, Department of Chemistry, P.O. Box 55 (A.I. Virtanens plats 1),

FIN-00014 University of Helsinki, Finland, Institute of Organic Chemistry, Polish Academy

of Sciences, Kasprzaka 44-52, 01-224 Warsaw, Poland, Schulich Department of Chemistry

Technion, Haifa 3200008, Israel, and University of Helsinki, Department of Chemistry,

P.O. Box 55 (A.I. Virtanens plats 1), FIN-00014 University of Helsinki, Finland.

E-mail: michal.jaszunski@icho.edu.pl; stanger@technion.ac.il; dage.sundholm@helsinki.fi

───────────────────

*To whom correspondence should be addressed

[†]University of Helsinki, Department of Chemistry, P.O. Box 55 (A.I. Virtanens plats 1), FIN-00014 University of Helsinki, Finland

[‡]Institute of Organic Chemistry, Polish Academy of Sciences, Kasprzaka 44-52, 01-224 Warsaw, Poland

[¶]Schulich Department of Chemistry Technion, Haifa 3200008, Israel

[§]University of Helsinki, Department of Chemistry, P.O. Box 55 (A.I. Virtanens plats 1), FIN-00014 University of Helsinki, Finland.

January 8, 2020

Abstract

The aromaticity of three non-planar, fully conjugated aza-nanographenes built around a pyrrolo[3,2-*b*]pyrrole core is assessed through application of two different computational procedures – GIMIC and NICS. We examine the calculated magnetically induced current densities (GIMIC) and nucleus independent chemical shifts (NICS). The structural differences between these three apparently similar molecules lead to significantly different aromatic properties. GIMIC analysis indicates that the peripheral diatropic ring current of 3.9 nA/T for the studied bowl-shaped diaza-nanographene is the strongest, followed by the double [6]helicene which lacks seven-membered rings, and is practically nonexistent for the double [5]helicene possessing seven-membered rings. The biggest difference however is that in the two not-fully-fused molecules the central pyrrole rings possess a significant diatropic current of about 4.1 nA/T, whereas there is no such current in the diaza-nanographene. Moreover, the antiaromaticity of the seven-membered rings is increasing while moving from double [5]helicene to diaza-nanographene (from -2.4 to -6.0 nA/T). The induced currents derived from $NICS_{\pi,zz}$-XY-scan analysis for all of the studied systems are in qualitative agreement with the GIMIC results. Subtle differences may originate from σ-electron currents in GIMIC or inaccuracy of $NICS_{\pi,zz}$ values due to the non-planarity of the systems, but the general picture is similar.

1 Introduction

Aromaticity has been a key idea in the development of organic chemistry over the past 150 years. It is not a well-defined concept even when one considers isolated rings, and it becomes more complicated for polycyclic aromatic hydrocarbons and their heterocyclic analogs. Numerous computational approaches have been employed to find out whether such a molecule is aromatic as a whole and, more importantly, to investigate the aromatic

character of various rings in the same polycyclic molecule.[1–28]

Aromatic properties of existing molecules and not yet synthesized compounds have been studied using these methods. The calculations suggest that while planar polycyclic aromatic hydrocarbons (PAHs) comprised of only six-membered rings often behave predictably, the presence of additional five and seven-membered rings makes the aromatic properties more complicated and interesting.[29–33] In particular, the incorporation of five-membered non-heterocyclic rings typically leads to antiaromaticity.[34] Decorating nanographenes with seven-membered rings is less common and a limited number of cases has been reported so far.[35–40] In principle, the propensity of the nitrogen atom to form three covalent bonds can enable the study of nanographene analogs in which the central benzene ring or naphthalene moiety is formally replaced with an aza-heterocyclic scaffold. Very recently, we succeeded in the surface-assisted synthesis of such a nitrogen-embedded buckybowl (diaza-nanographene, molecule **1** in Figure 1), possessing two seven-membered rings, two five-membered rings, 10 six-membered rings and a fully conjugated structure.[41] The presence of two fused pyrrole rings in this molecule offers unique opportunities that did not previously exist for the investigation of curved aromatic systems. Thus, the key question behind this work is how the aromatic properties of nanographene analogs will be affected by the concave curvature and the presence of pyrrole rings adjacent to seven-membered rings.
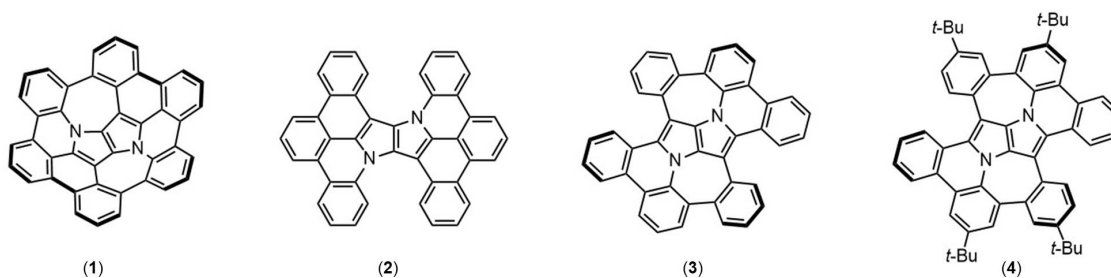
Figure 1: The molecular structures of bowl-shaped diaza-nanographene (**1**), double [6]helicene (**2**), double [5]helicene (**3**) and substituted double [5]helicene (**4**).

There is a variety of theoretical methods that enable the study and interpretation of molecular magnetic properties, related to their aromatic or antiaromatic character.[42–44]

Given that aromaticity of curved molecules containing pyrrole units is very rarely studied, [45] in this work we examine the properties of four previously synthesized [41] curved molecules shown in Figure 1. The aromaticity of these non-planar molecules, consisting of increasing numbers of 5-, 6- and 7-membered rings, will be first discussed in terms of the net dia- and paratropic ring currents induced by the magnetic field perpendicular to the central diaza-pentalenic unit. In addition to the ring currents, we also present the values of nucleus independent chemical shifts (NICS). We determine the aromatic or antiaromatic character of all the rings using the NICS-scan procedure.

2 Computational methods

2.1 GIMIC

The magnetically induced current density (susceptibilities) and strengths of the current density (susceptibilities) were computed using the open-source GIMIC program. [42,46–48] The input data for the GIMIC program are basis-set information, density matrices and magnetically perturbed density matrices, which are obtained in calculations of nuclear magnetic resonance (NMR) shielding constants. The NMR shielding constants were calculated with the Turbomole program package version 7.3 [49,50] at the density functional theory (DFT) level using Becke's three-parameter functional (B3LYP) [51–53] with the Karlsruhe triple-ζ quality basis sets (def2-TZVP). [54] Gauge-including atomic orbitals (GIAO) were applied in order to ensure gauge-origin independence and a fast basis-set convergence for the current density. [55–57] The strengths of the current density along different current pathways were obtained by integrating the current density flow passing planes that intersect chemical bonds perpendicularly to it. [46] In the figures we shall use black arrows to show the path for the global current, pink and red arrows to show the dia- and paratropic currents in the sub-rings, and green arrows to show currents which contribute, but do not sustain a current in the sub-rings.

The molecular structures (given in the Supporting Information) were optimized using

B3LYP. Dispersion was considered with Grimme's D3-BJ correction[58] and def2-TZVP basis sets were employed. The calculations were performed with Turbomole version 7.3.

2.2 NICS

Different NICS-based approximations are used to study aromaticity; we refer to a recent review[43] for a description and to other recent works[59–62] for examples of applications.

The NICS-XY-scan approximation applied in this work was developed in order to allow the study of polycyclic systems using the NICS approach. In these systems, several types of ring currents are possible: local (at each ring), semi-global (on two or more rings) and global (spreading over or around the whole system). In many cases, two or more of such currents are overlapping. Hence, regular NICS procedures which produce values above the center of the rings represent the magnetic field that is induced by all the currents below it, therefore give only a partial, sometimes misleading picture of the tropicity of the studied systems. The NICS-XY-scan procedure is based on the fact that following a trajectory along which NICS values are computed allows deduction of the ring current(s) which produce this induced magnetic field, as manifested by the NICS value.[63] The detailed rules for the interpretation of the NICS-scan trajectories are given elsewhere,[64] but in short, a maximum/minimum with a positive/negative NICS value represents the center of diatropic/paratropic current, respectively and a shoulder represents a point in which two (or more) currents start to overlap.

For aromaticity purposes, the π-system is best described by $NICS_{\pi,zz}$ values, namely, the zz part of the shielding tensor (perpendicular to the molecular plane) for which only the contribution of the π electrons is considered. These can be obtained by two different procedures: Canonic Molecular Orbitals (CMO-$NICS_{\pi,zz}$) and the σ-only model (σ-only-$NICS_{\pi,zz}$).[65] The CMO-NICS method requires a clear separation between the σ and π electrons, therefore it can be applied only for planar systems. Since most of the systems that are studied here are not planar, the σ-only-$NICS_{\pi,zz}$ is used for all the calculations. It should be noted

that direct comparison between $\mathrm{NICS}_{\pi,zz}$ and GIMIC results is not straightforward. Thus, while $\mathrm{NICS}_{\pi,zz}$ describes the magnetic field created by ring currents originating from the π electrons only, GIMIC considers both π and σ electrons.

NICS calculations were carried out using the Aroma software[66] at the GIAO-B3LYP-6-311+G(d) computational level (for B3LYP/6-311G(d) optimized molecular structures). $\mathrm{NICS}(1)_{\pi,zz}$ values were obtained from NICS-scan[67] and the σ-only procedure[65] (CMO-$\mathrm{NICS}_{\pi,zz}$ values cannot be obtained since the molecules are not planar). The NICS-XY-scan procedure[63] at a distance of 1.7 Å above the rings was used for identifying local, semi-global and global π currents.

3 Results and discussion

3.1 Molecule 2

3.1.1 GIMIC

The strengths of the current density passing selected chemical bonds of **2** are shown in Figure 2, where one sees that the benzene rings at the periphery of the molecule sustain weak local diatropic ring currents. The strengths of their local diatropic ring currents are in the range of 2.6 – 5.4 nA/T. The inner benzene rings do not sustain any local ring current. They serve as bridges allowing the current density flow between the two annelated pyrrole rings to the outer benzene rings, as shown with the green arrows. A diatropic ring current flows along the edge around the whole molecule. The strength of the current density along the perimeter, shown with black arrows in Figure 2, is 9.2 nA/T in the left part of the molecule. The edge current splits at the nitrogen of the pyrrole rings leading to a weaker edge current of 3.4 nA/T at two of the outer benzene rings. A current pathway of about 9 nA/T follows the outer bonds of the two annelated pyrrole rings and splits into two almost equally strong pathways leading to a local ring current of 3.5 nA/T around the two pyrrole

rings. Kirchhoff's law for charge conservation is not completely fulfilled due to difficulties in the determination of the integration domains.
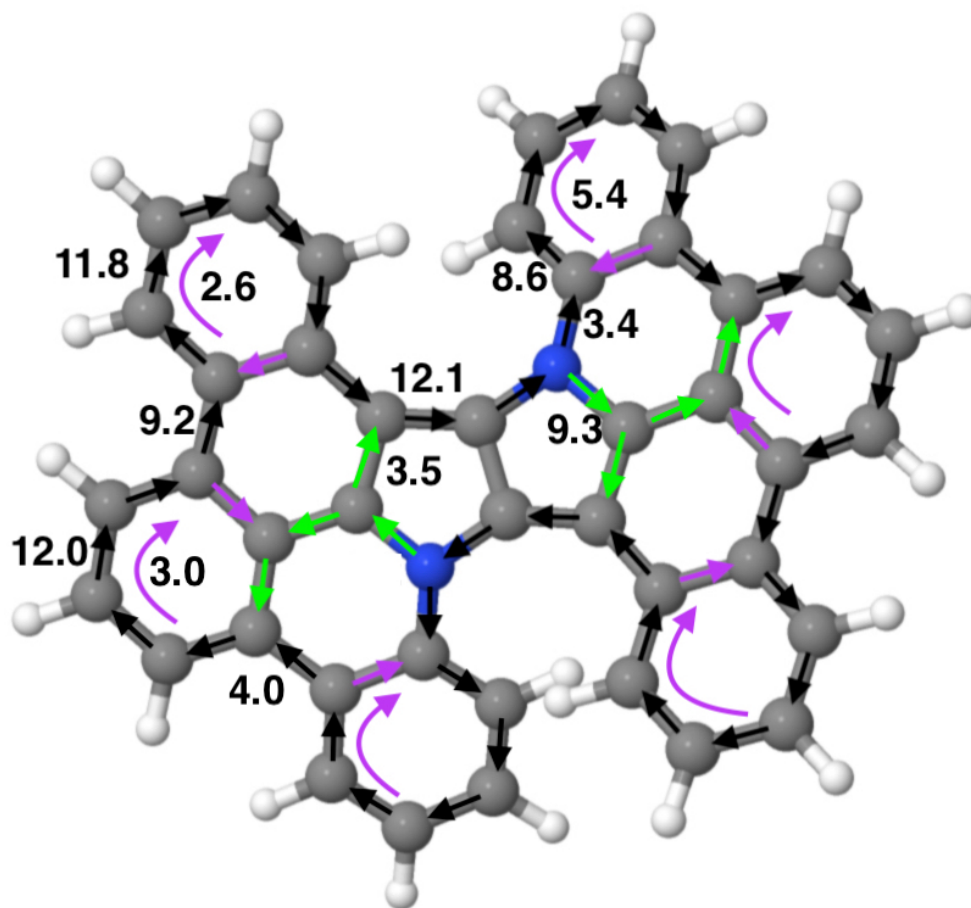

Figure 2: The strength of the current density passing selected chemical bonds of **2** calculated using the GIMIC program.

3.1.2   NICS

Molecule **2** is built from two parts which are not co-planar, but each is planar. The interpretation of the scan curves is therefore simple. Figure 3 gives the labelling of **2** used for the $NICS_{\pi,zz}$ scans shown in Figure 4. The scan 4a clearly shows a semi-global current on the two five-membered rings (B and C), centered on bond d. Rings A and D are diatropic, and from scan 4b it seems that they are local. Scan 4b suggests a local current at ring E (and in its symmetric equivalent) and no current at ring F. Rings G and H and their symmetric
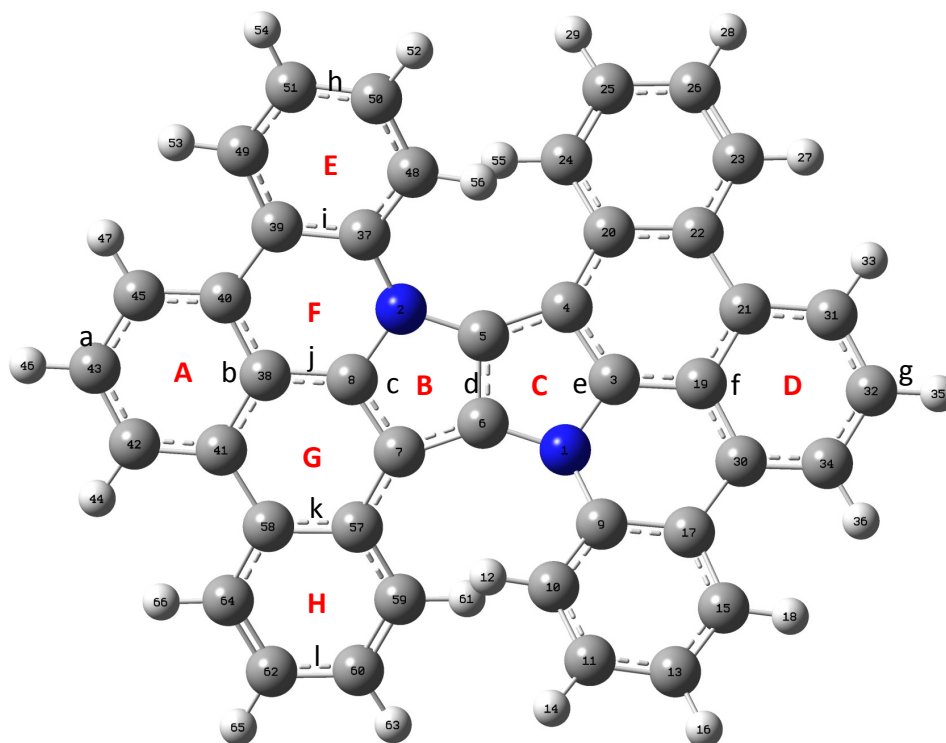
Figure 3: Labelling of molecule **2** applied in the analysis of the NICS scans.
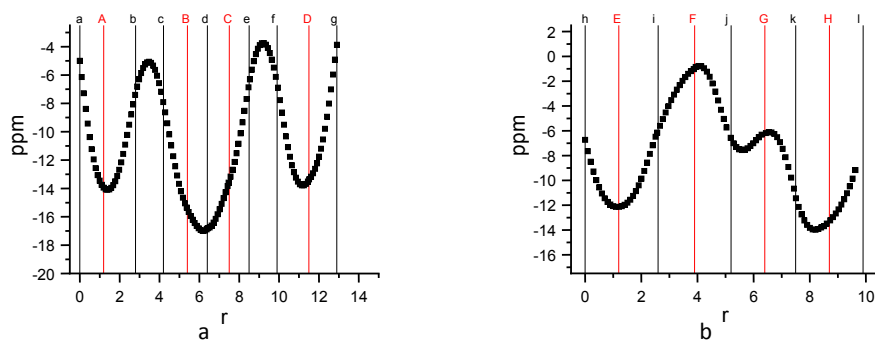
1
2
3
4
5
6
7
8
9
10
11
12
13
14
15
16
17
18
19
20
21
22
23
24
25
26
27
28
29
30
31
32
33
34
35
36
37
38
39
40
41
42
43
44
45
46
47
48
49
50
51
52
53
54
55
56
57
58
59
60

Figure 4: $\mathrm{NICS}_{\pi,zz}$-XY-scans of **2** (see Figure 3).

equivalents seem to share a semi-global diatropic current, with an additional local current at ring H.

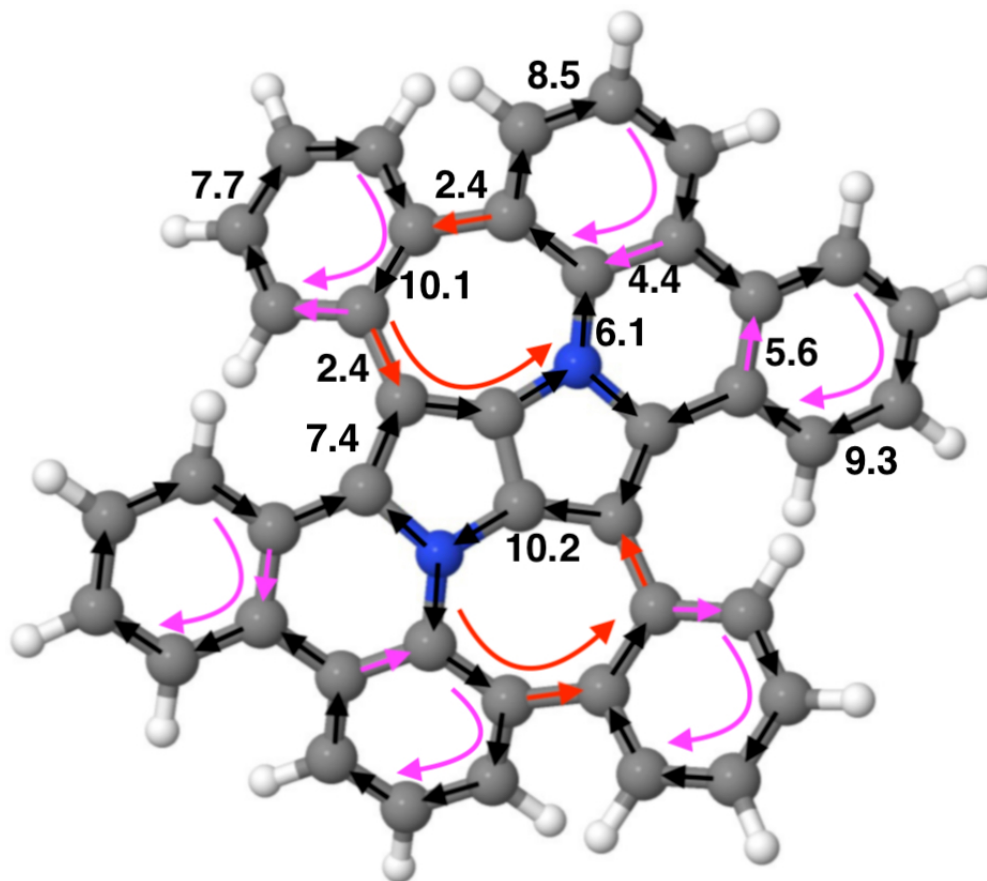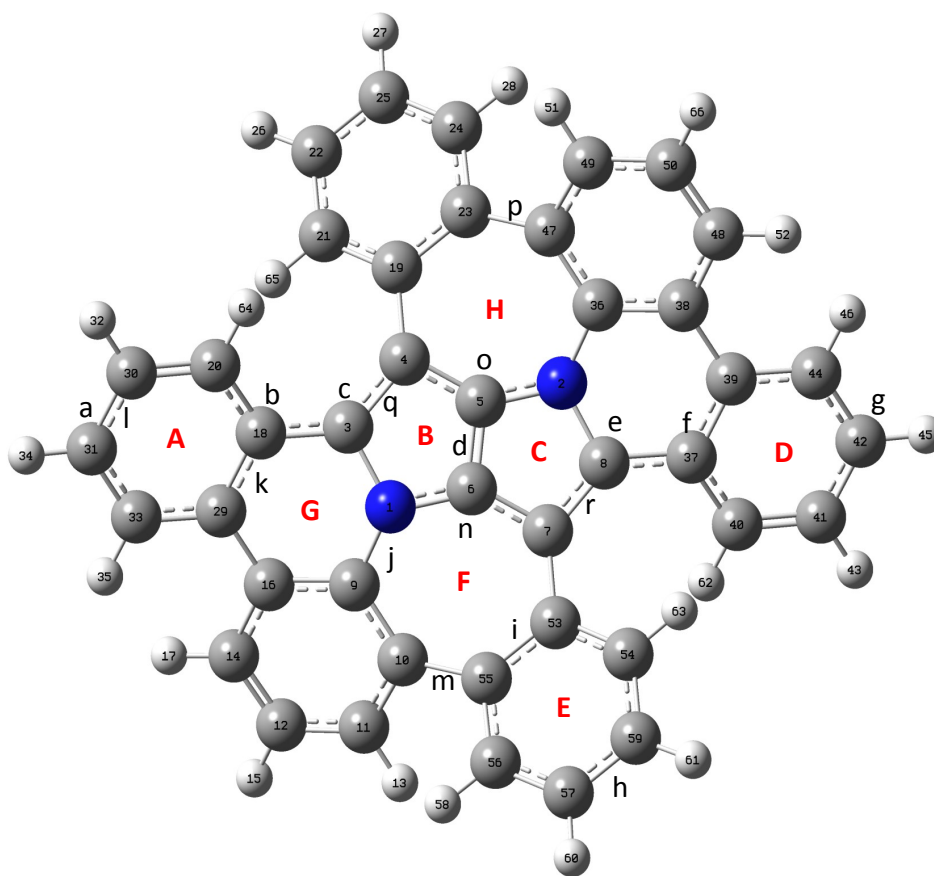## 3.2 Molecule 3

3.2.1 GIMIC

Figure 5: The strength of the current density passing selected chemical bonds of **3** calculated using the GIMIC program.

The strengths of the current density passing selected chemical bonds in **3** are shown in Figure 5, where one sees that the benzene rings at the periphery of the molecule sustain local diatropic ring currents, with strengths of 4.4, 5.6 and 7.7 nA/T. Analogously to **2**, the inner benzene rings serve as bridges allowing the current density flow between the two pyrrole rings and the outer benzene rings. There is no significant edge current around the whole

molecule **3**. The current density flow in the rings annelated to the seven-membered rings results in a weak paratropic ring current of -2.4 nA/T in the heptagon. A current pathway of 10.2 nA/T follows the common bonds of the seven-membered ring and the two annelated pyrrole rings and splits at the nitrogens into two pathways, whose strengths are 6.1 nA/T and 4.1 nA/T, respectively, implying that the annelated pyrrole rings sustain a local ring current of 4.1 nA/T.

3.2.2 NICS

Figure 6: Labelling of molecule **3** applied in the analysis of the NICS scans.

Molecule **3** is very difficult to analyze due to its non-planarity and the fact that some individual rings are not planar as well. This causes asymmetry in the scan curve which should otherwise be symmetric; many of these complications are due to the structure of the
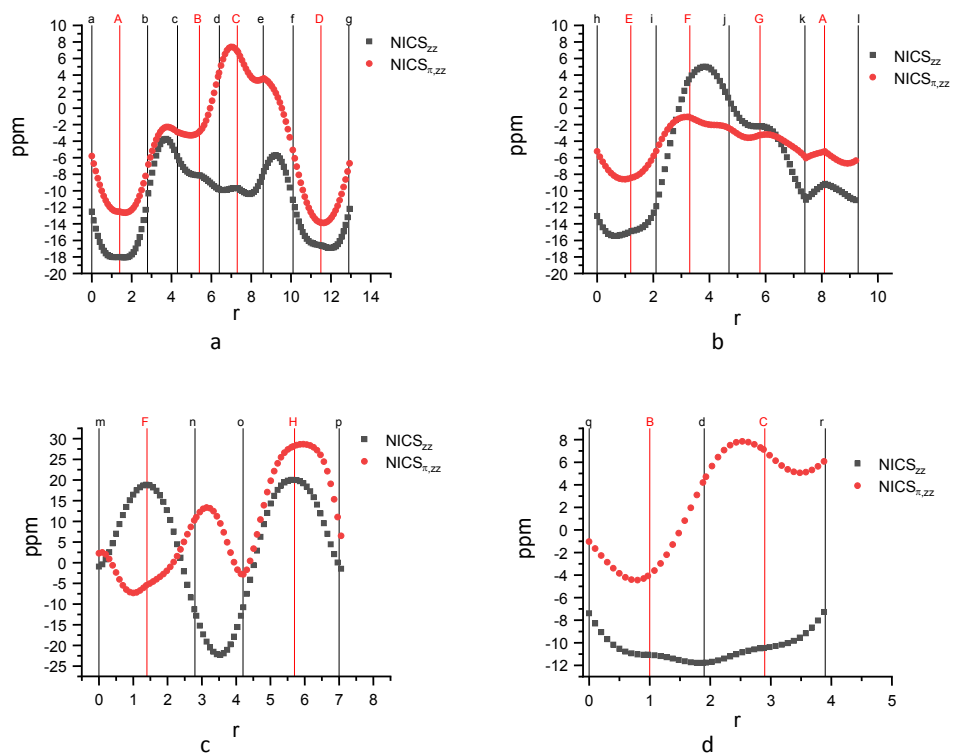
Figure 7: $NICS_{\pi,zz}$ and $NICS_{zz}$ -XY-scans of **3** (see Figure 6).

σ-only model. The scan is performed 1.7 Å above the molecular plane, since at this distance the shape (but not the values) of the $NICS_{zz}$ scan is similar to that of the $NICS_{\pi,zz}$ scan.[63] Figures 6 and 7 show the labelling and the $NICS_{zz}$ and $NICS_{\pi,zz}$ scans of **3**, respectively. The analysis is qualitative, since there are sometimes significant differences between the $NICS_{zz}$ and the $NICS_{\pi,zz}$ scans.

Figures 7a and 7b suggest that rings A and E are diatropic and that their diatropic currents are local. From Figure 7a and the region between n and o in Figure 7c it looks like rings B and C share a semi-global diatropic current. From Figure 7b and especially Figure 7c it is clear that both seven-membered rings F and H are paratropic. Ring G is non-aromatic. since its NICS value is ≈ 0, as seen in Figure 7b.

3.2.3   NMR of molecule 4 − tetrakis(t-Bu)-substituted molecule 3

The first computational step of the two approaches we use to analyse aromaticity provides the shielding constants of all the nuclei, which can be compared with experimental data to estimate the quality of the employed computational methods. For **4**, we can compare the experimental and computed NMR chemical shifts. The spectrum has been measured for **4**, because it possesses sufficient solubility for 2D NMR studies, whereas **3** is almost insoluble in all common solvents. Molecule **1** has so far been prepared only via surface assisted synthesis using scanning tunneling microscope (STM), which precludes NMR characterization; NMR data for molecule **2** has already been reported.[68] We do not discuss the current density of **4**, because it is practically the same as that of **3**.

Figure 8 shows the agreement between the computed (B3LYP/def2-TZVP, see above) and observed aromatic carbon chemical shifts. The agreement of the calculated chemical shifts and the experimental data is satisfying with a slope of 0.93 and an offset of 3.17 in the regression analysis; the R^2 coefficient of the fit is 0.97. A similar regression analysis shows that the calculations generally overestimate the ^1H NMR chemical shifts, whereas the linear correlation indicates that the employed computational level provides a reliable description of

the magnetic-field induced currents. The calculated and measured ^{13}C NMR and ^{1}H NMR chemical shifts are described in more detail in the Supporting Information.
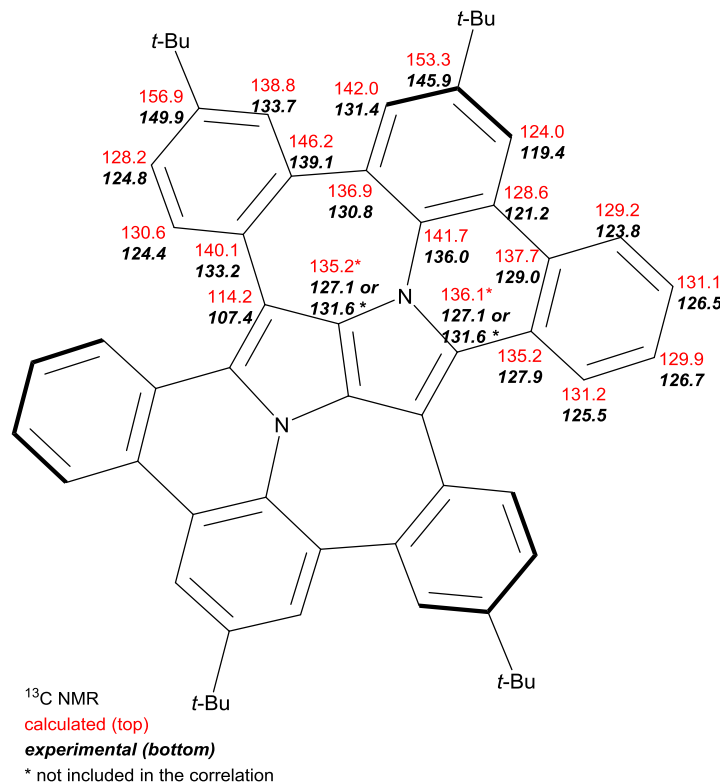

Figure 8: The computed and observed aromatic carbon chemical shifts in **4**. The asterisks denote the shifts of two carbon nuclei which cannot be assigned from the spectrum.

3.3   Molecule 1

3.3.1   GIMIC

The current density flow and the strength of the current density passing selected bonds of **1** are shown in Figure 9. Four of the benzene rings along the edge of the molecule sustain local diatropic ring currents, with strengths of 3.7 nA/T (12.0–8.3 and 7.6–3.9 nA/T) and two of the benzene rings sustain a very weak ring current of 0.7 nA/T. The inner benzene rings do not sustain any local ring currents. They constitute bridges for ring-current flow
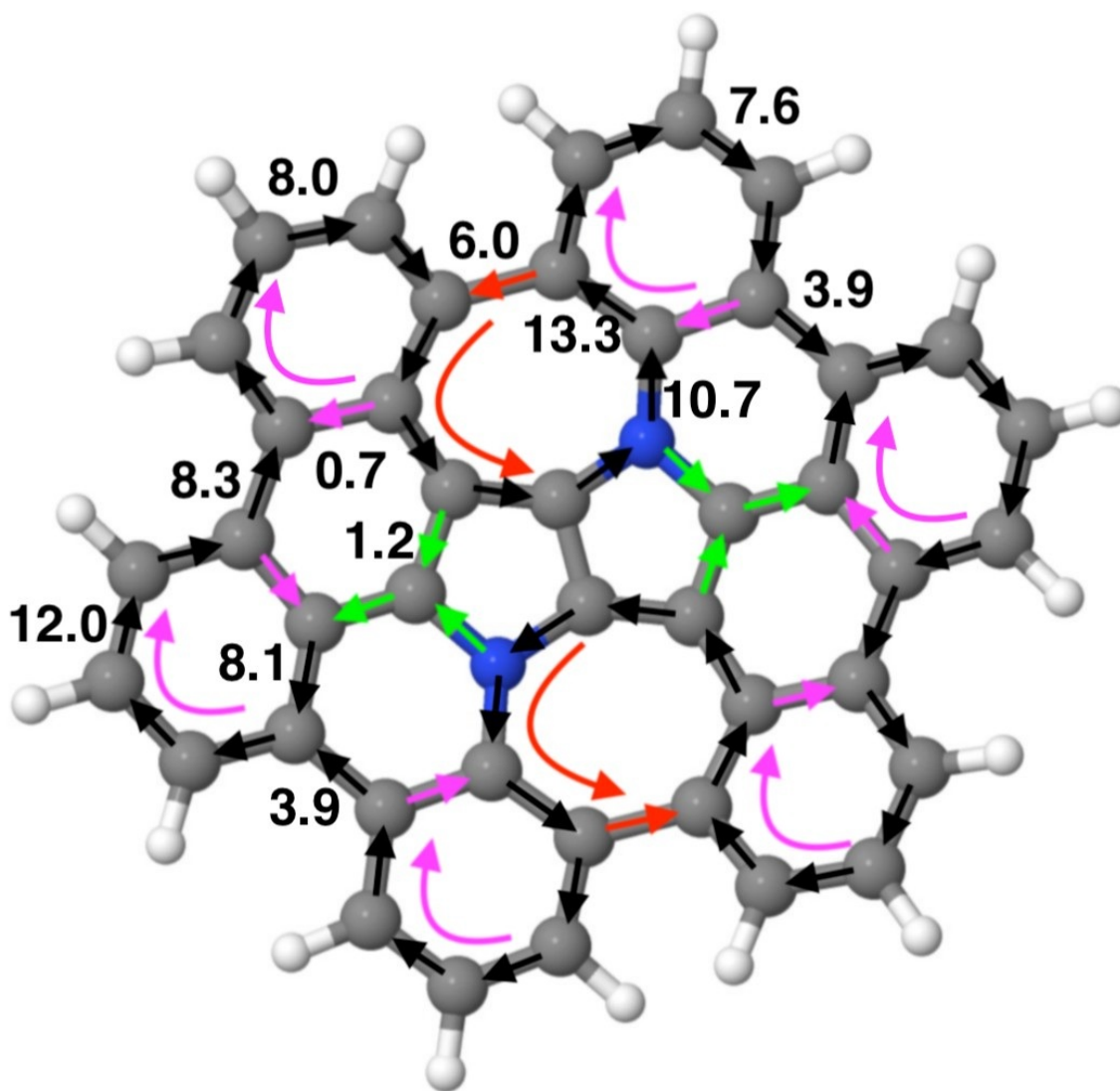
Figure 9: The strength of the current density passing selected chemical bonds of **1** calculated using the GIMIC program.

in the neighboring rings. The annelated pyrrole rings do not sustain any local ring current, as shown by the green arrows. They only function as bridges for the main ring current flow that goes along the outer edge of the molecule and turns inside at the seven-membered ring, which sustains a local paratropic ring current of -6.0 nA/T. The strength of the global ring current shown with black arrows is 3.9 nA/T.

3.3.2 NICS

Since molecule **1** is non-planar the NICS_{zz} scans are included. However, in contrast to **3**, in most cases the shape of the NICS_{zz} scans (see Figures 10 and 11) are similar to the respective scans of $\text{NICS}_{\pi,zz}$, confirming the results.

Figure 11a has the same basic features as the respective scans of **2** and **3**, suggesting local diatropic currents at rings A and D and a semi-global diatropic current in B and C. Figure 11b has the same features as the respective scan in **3** (Figure 7c), indicating local paratropic currents at the seven-membered rings E and F. Figure 11c suggests similar conclusions to that of Figure 7b (please note that the direction of the trajectory is opposite), suggesting a local diatropic current at rings A and H, paratropic current at E and no current at G. Figure 11d is a mirror image of Figure 4b (due to the opposite direction of the scan trajectory), suggesting local diatropic current at ring I, no current in ring G, and a local diatropic loop at ring K.

A global π current passing through the bonds h and k is not possible because rings E and F are paratropic, while all the other rings at the circumference are diatropic. This is verified by the circumference scan I-H-D-I′-K-A (Figure 11e*), demonstrating both the paratropicity of the bonds belonging to the seven-membered ring and the localized nature of the diatropic currents in the other rings. However, a global current such as shown in Figure 9 – excluding bonds h and k of the seven-membered rings which directly link the six-membered rings – is feasible, in particular when we also consider the σ electrons.

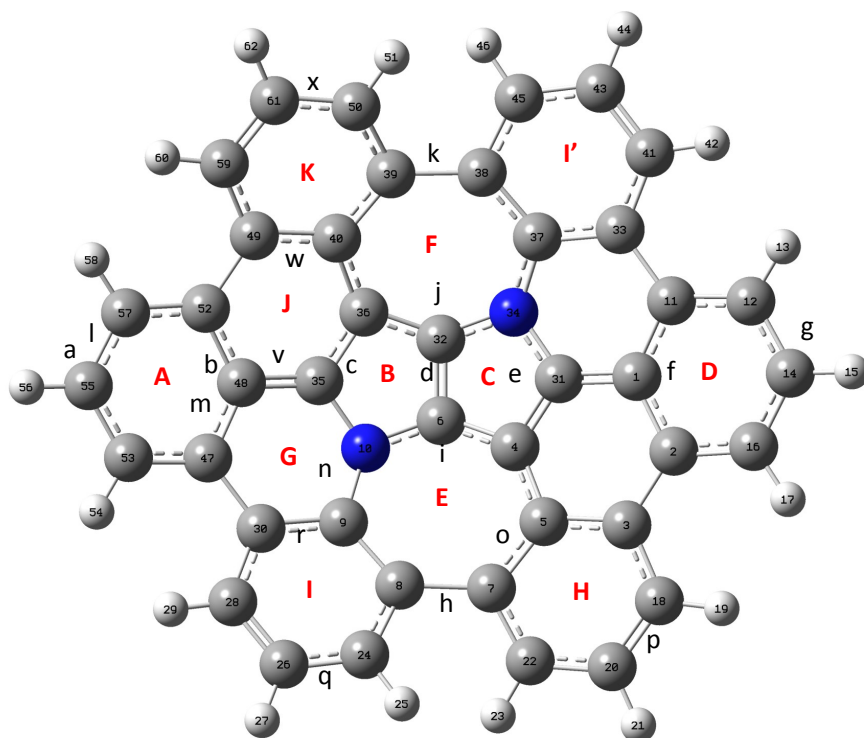A somewhat analogous trend has been observed for a highly distorted azananographene

Figure 10: Labelling of molecule **1** applied in the analysis of the NICS scans.
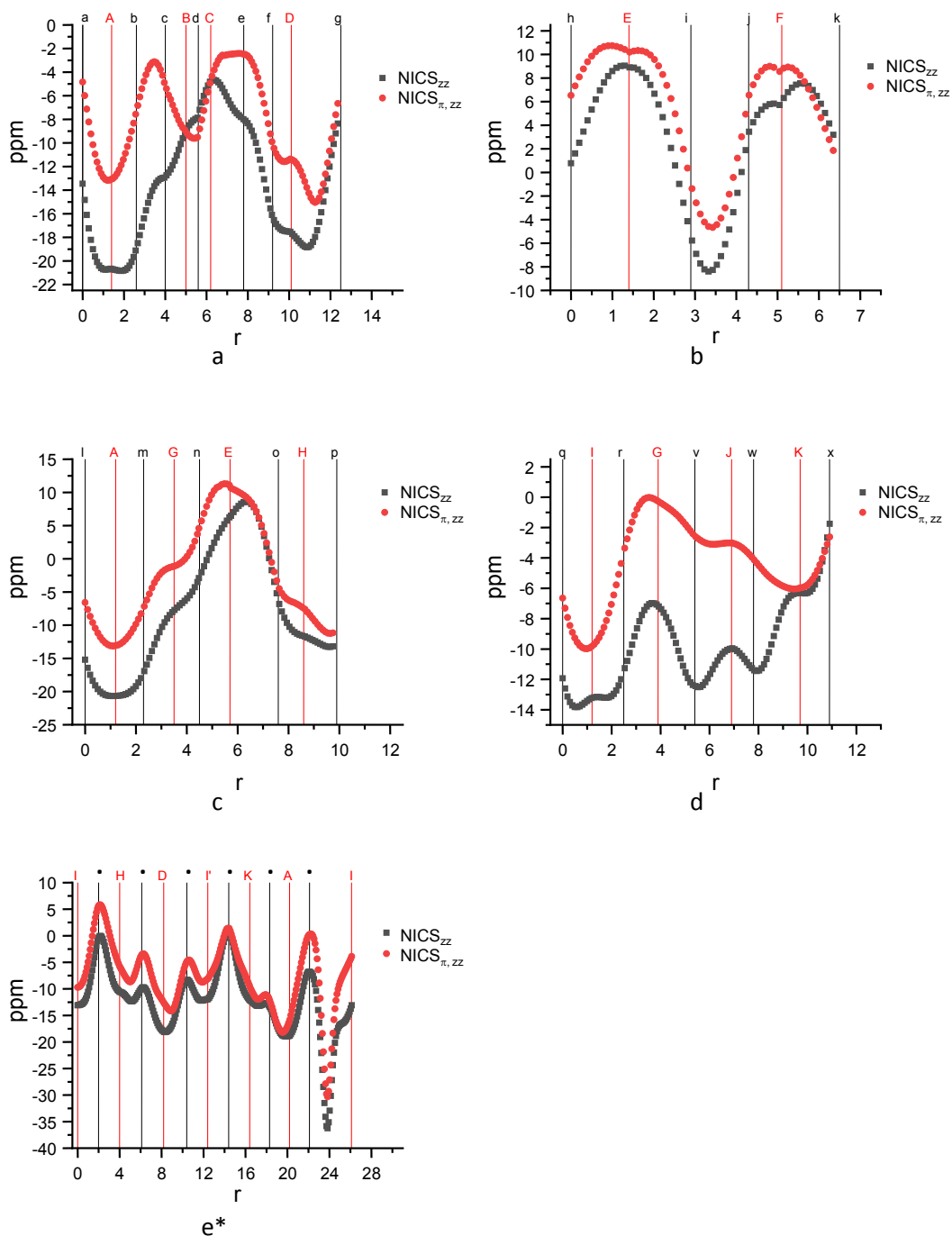
Figure 11: $NICS_{\pi,zz}$ and $NICS_{zz}$-XY-scans of 1 (see Figure 10).
e*: Periphery scan between the center of the rings (red capital letter) and the center of the bond connecting two adjacent rings (·).

composed of eight conjugated pyrrole rings.[45] Peripheral pyrrole rings are aromatic (negative NICS values), while seven-membered rings possess antiaromatic character. In addition, the naphthalene moiety located at the center of the molecule has aromatic character, in analogy to the central pyrrolo[3,2-b]pyrrole in bowl **1**. Very recently, Tokimaru *et al.* synthesized a highly curved buckybowl containing an internal nitrogen atom.[69] The NICS(0) analysis indicated a significant decrease in the antiaromaticity of the central five-membered ring of the aza-bowl shaped molecule compared to the corresponding part of corannulene.

3.4   Comparison with polycyclic aromatic hydrocarbons

3.4.1   GIMIC

The current density pathways of molecules **1**-**3** are compared to those in polycyclic aromatic hydrocarbons (PAHs) of a similar size, such as ovalene and hexabenzocoronene, which are known to have different current-density pathways.

The current density flow in ovalene (Figure 12) is dominated by a strong diatropic edge current of 15.5 nA/T around the molecule.[21] The benzene rings at both ends of the molecule and those in the middle of the two sides of ovalene are Clar rings[70,71] sustaining a local ring current of about 6 nA/T, whereas the other benzene rings do not sustain any local ring currents. They are bridging rings rendering the local ring currents feasible.

For comparison with molecules **1**-**3** we have in addition performed calculations at the B3LYP/def2-TZVP/D3-BJ level on hexabenzocoronene. The results show that hexabenzo-coronene sustains a global ring current of 7.3 nA/T (Figure 13). The six outer Clar rings of hexabenzocoronene sustain local ring currents of 6.3 nA/T, which are slightly weaker than the global ring current along the outer edge of the molecule. The Clar ring in the center of hexabenzocoronene sustains a local ring current of 12.0 nA/T. The current strengths and pathways are in good agreement with the results obtained in previous studies.[46,72]

The calculations show that it is difficult to find a simple rule that can be applied to all PAHs. However, they generally sustain a strong diatropic ring current along the perimeter
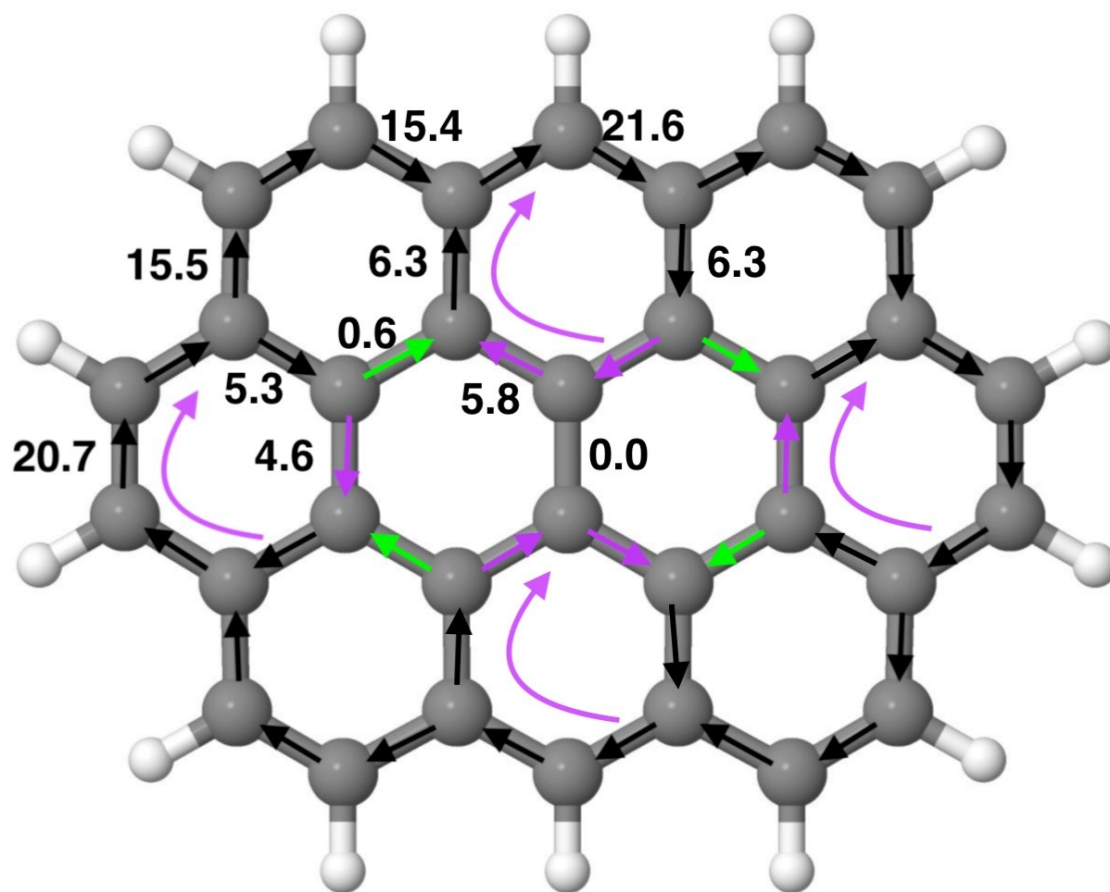
Figure 12: The strength of the current density passing selected chemical bonds of ovalene. The current strengths are taken from M. Kaipio *et al.*, *J. Phys. Chem. A* **2012**, *116*, 10257-10268.
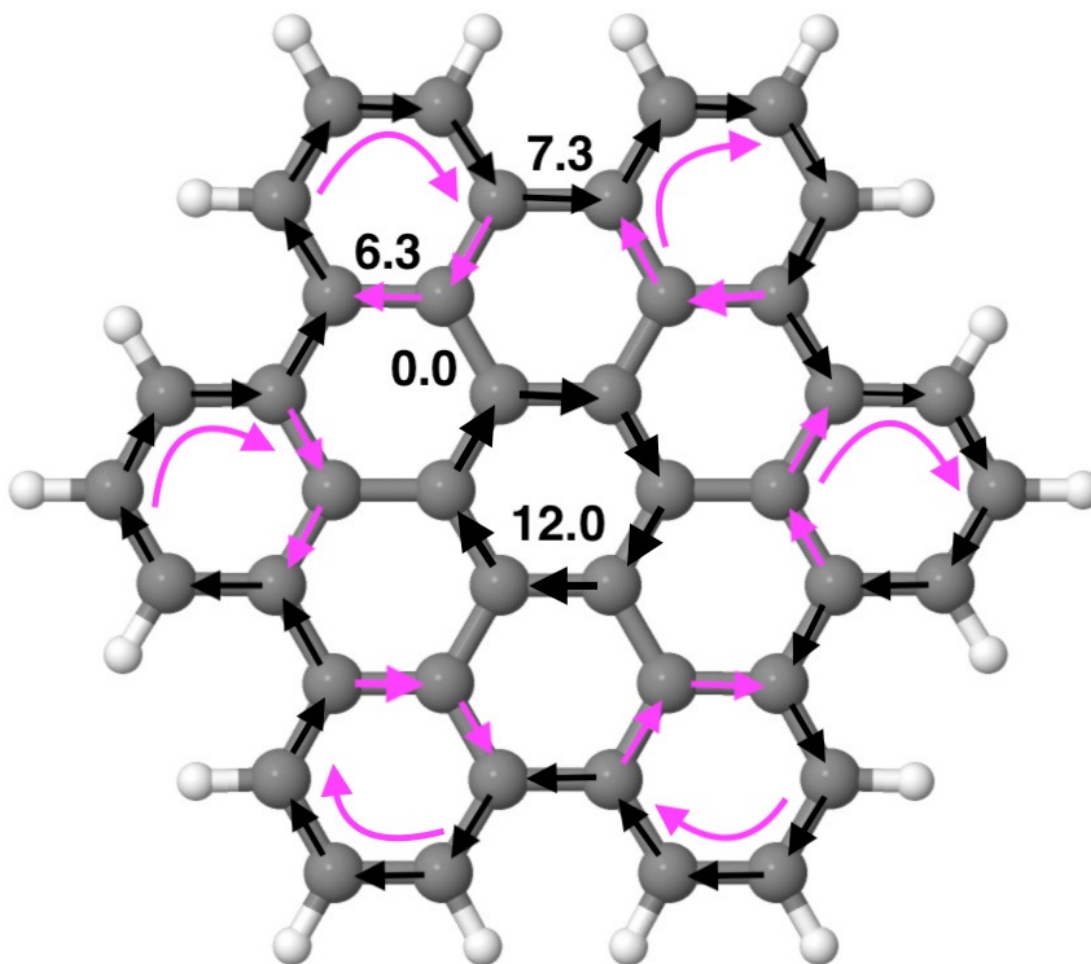
Figure 13: The strength of the current density passing selected chemical bonds of hexaben-zocoronene calculated at the B3LYP/def2-TZVP level.

of the whole molecule, whereas the individual hexagons can sustain a rather strong local ring current, a weak ring current or no ring current at all depending on their position and the topology of the molecule. The current pathways of molecules **1**-**3** differ from the ones for the studied PAHs. The global ring current along the perimeter is weak in comparison to the PAHs. The heptagons in **1** sustain local paratropic ring currents in harmony with the global diatropic ring current passing on the inside of the seven-membered ring. The benzene rings along the edge of the molecule are Clar rings sustaining weak local ring currents. The rest of the rings functions as bridges. The same current pattern is obtained for molecule **3**. The main difference is that in **3** a local ring current flows around the two annelated pyrrole rings. The current strengths in the Clar rings are stronger and the paratropic ring current in the heptagons of **3** is weaker than in **1**. The current pathway in **2** shows that the six Clar rings sustain relatively weak local ring currents. The global ring current and the local ring current around the two annelated pyrrole rings are of the same strength as for **1** and **3**, respectively.

The pattern of the current pathway in **2** is to some extent similar to the one for ovalene, whereas for **3** the current pathways are more reminiscent of the ones for hexabenzocoronene. Due to the strong local paratropic ring currents in **1**, the current density pattern differs from the ones of the PAHs.

3.4.2   NICS

The labelling and the NICS-XY-scans of ovalene are presented in Figures 14 and 15. Scan 15a suggests a diatropic ring current over the whole anthracenic unit and additional diatropicity in ring B. Scan 15b suggests diatropicity at rings D and G and shows a maximum over the center (g). These data indicate a global ring current at the outer rings and local ring currents at B and D (and their symmetric equivalent rings), with the current at D somewhat stronger than at B. Figures 15c and 15d confirm this pattern of the currents. We note that the maximum at g in scan 15b has a negative value and is a result of the global ring current.
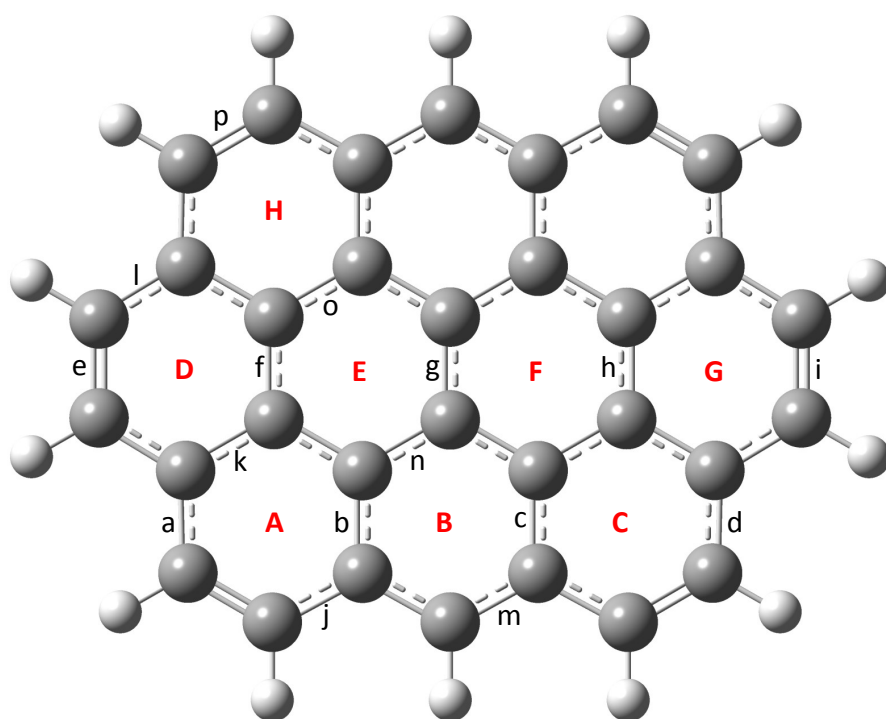
Figure 14: Labelling of ovalene applied in the analysis of the NICS scans.

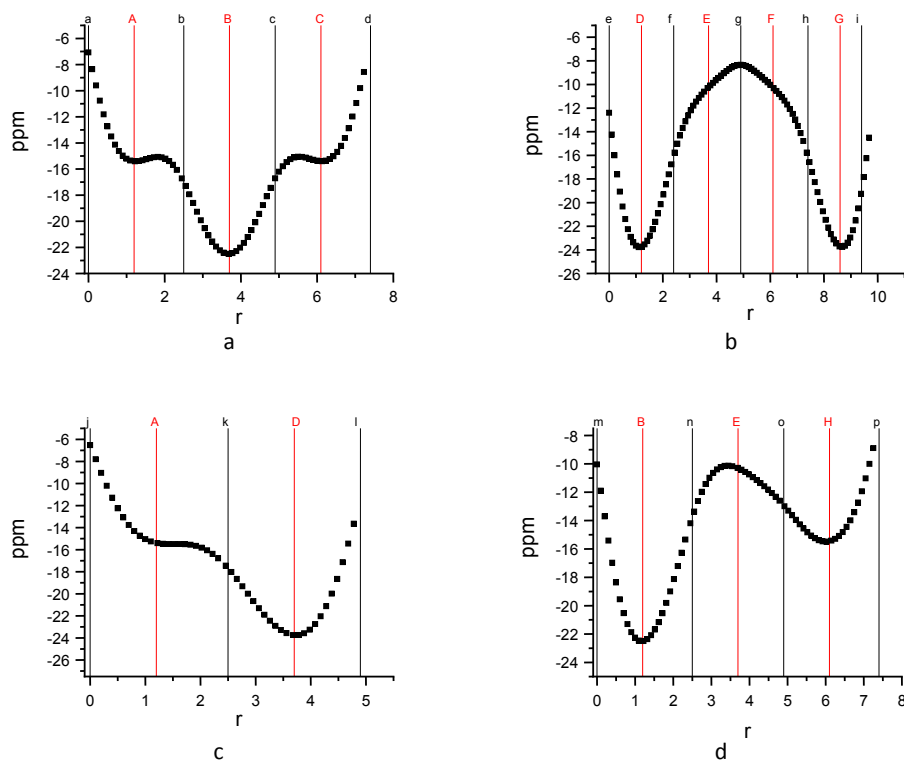Figure 15: $\text{NICS}_{\pi,zz}$-XY scans of ovalene (see Figure 14).

4   Conclusions

While the aromaticity of several curved architectures has been investigated lately, we present here the first case of such a study investigating a bowl-shaped molecule possessing hetero-cyclic rings at its center. The analysis of three structurally related molecules enabled us to elucidate how the formation of two single bonds, the presence of seven-membered rings and/or the curvature influence the local and global aromaticity. In contrast to the somewhat analogous hexabenzocoronene and ovalene, in the N-doped curved nanographene the diatropic edge current is relatively weak.

The formal transformation of double helical aza-nanographenes into bowl-shaped aza-nanographene is associated with large changes in the aromaticity. Seven-membered rings become more antiaromatic, while the central five-membered pyrrole rings which in the case of double [5]helicene and double [6]helicene supported a diatropic current, serve only as bridges in the buckybowl. The presence of seven-membered rings makes the two molecules less aromatic compared to the regioisomer possessing six-membered and five-membered rings only.

5   Supporting information

Molecular structures; Figure S1 – computed and observed aromatic carbon chemical shifts in **4**; Figure S2 – computed and observed aromatic proton chemical shifts in **4**.

Acknowledgement

References

(1) Poater, J.; Solà, M.; Viñas, C.; Teixidor, F. π Aromaticity and Three-Dimensional Aromaticity: Two Sides of the Same Coin? *Angew. Chem. Int. Ed.* **2014**, *53*, 12191–12195.

(2) Pierrefixe, S.; Bickelhaupt, F. Aromaticity: Molecular-Orbital Picture of an Intuitive Concept. *Chem. Eur. J.* **2007**, *13*, 6321–6328.

(3) Hill, J. G.; Cooper, D. L.; Karadakov, P. B. Spin-Coupled Description of Aromaticity in the Retro Diels–Alder Reaction of Norbornene. *J. Phys. Chem. A* **2008**, *112*, 12823–12828.

(4) Jorner, K.; Jahn, B. O.; Bultinck, P.; Ottosson, H. Triplet State Homoaromaticity: Concept, Computational Validation and Experimental Relevance. *Chem. Sci.* **2018**, *9*, 3165–3176.

(5) Poater, J.; Solà, M. Open-Shell Spherical Aromaticity: the $2N^2 + 2N + 1$ (with $S = N + 1/2$) Rule. *Chem. Commun.* **2011**, *47*, 11647–11649.

(6) Monaco, G.; Aquino, F.; Zanasi, R.; Herrebout, W.; Bultinck, P.; Massa, A. Model-Averaging of Ab Initio Spectra for the Absolute Configuration Assignment via Vibrational Circular Dichroism. *Phys. Chem. Chem. Phys.* **2017**, *19*, 28028–28036.

(7) Cyrañski, M. K.; Krygowski, T. M.; Wisiorowski, M.; van Eikema Hommes, N. J. R.; Schleyer, P. V. R. Global and Local Aromaticity in Porphyrins: An Analysis Based on Molecular Geometries and Nucleus-Independent Chemical Shifts. *Angew. Chem. Int. Ed. 37*, 177–180.

(8) Solá, M. Why Aromaticity Is a Suspicious Concept? Why? *Front. Chem.* **2017**, *5*, 22.

(9) Chen, Z.; Heine, T.; Sundholm, D.; von Ragué Schleyer, P. In *Quantum Chemical*

Calculation of Magnetic Resonance Properties; Kaupp, M., Bühl, M., Malkin, V., Eds.; Wiley-VCH: Weinheim, Germany, 2004; pp 395–407.

(10) Jusélius, J.; Sundholm, D. Polycyclic Antiaromatic Hydrocarbon. *Phys. Chem. Chem. Phys.* **2008**, *10*, 6630–6634.

(11) Aihara, J. Nucleus-Independent Chemical Shifts and Local Aromaticities in Large Polycyclic Aromatic Hydrocarbons. *Chem. Phys. Lett.* **2002**, *365*, 34–39.

(12) Stanger, A. What is... Aromaticity: a Critique of the Concept of Aromaticity–Can it Really be Defined? *Chem. Comm.* **2009**, 1939–1947.

(13) Soncini, A.; Fowler, P. W.; Lazzeretti, P.; Zanasi, R. Ring-Current Signatures in Shielding-Density Maps. *Chem. Phys. Lett.* **2005**, *401*, 164–169.

(14) Randic, M. Aromaticity of Polycyclic Conjugated Hydrocarbons. *Chem. Rev.* **2003**, *103*, 3449–3605.

(15) Poater, J.; Solá, M.; Viglione, R. G.; Zanasi, R. Local Aromaticity of the Six-Membered Rings in Pyracylene. A Difficult Case for the NICS Indicator of Aromaticity. *J. Org. Chem.* **2004**, *69*, 7537–7542.

(16) von Ragué Schleyer, P.; Jiao, H. What is Aromaticity? *Pure Appl. Chem.* **1996**, *28*, 209–218.

(17) Fias, S.; Fowler, P. W.; Delgado, J. L.; Hahn, U.; Bultinck, P. Correlation of Delocalization Indices and Current-Density Maps in Polycyclic Aromatic Hydrocarbons. *Chem. Eur. J.* **2008**, *14*, 3093–3099.

(18) Fliegl, H.; Sundholm, D.; Taubert, S.; Jusélius, J.; Klopper, W. Magnetically Induced Current Densities in Aromatic, Antiaromatic, Homoaromatic, and Nonaromatic Hydrocarbons. *J. Phys. Chem. A* **2009**, *113*, 8668–8676.

(19) Fowler, P. W.; Myrvold, W. The Antracene Problem: Closed-Form Conjugated-Circuit Models of Ring Currents in Linear Polyacenes. *J. Phys. Chem. A* **2011**, *115*, 13191–13200.

(20) Fliegl, H.; Sundholm, D. Aromatic Pathways of Porphins, Chlorins and Bacteriochlorins. *J. Org. Chem.* **2012**, *77*, 3408–3414.

(21) Kaipio, M.; Patzschke, M.; Fliegl, H.; Pichierri, F.; Sundholm, D. The Effect of Fluorine Substitution on the Aromaticity of Polycyclic Hydrocarbons. *J. Phys. Chem. A* **2012**, *116*, 10257–10268.

(22) Fowler, P. W.; Steiner, E.; Havenith, R. W. A.; Jenneskens, L. W. Current Density, Chemical Shifts and Aromaticity. *Magn. Reson. Chem.* **2004**, *42*, S68–S78.

(23) Fliegl, H.; Özcan, N.; Mera-Adasme, R.; Pichierri, F.; Jusélius, J.; Sundholm, D. Aromatic Pathways in Thieno-Bridged Porphyrins: Understanding the Influence of the Direction of the Thiophene Ring on the Aromatic Character. *Mol. Phys.* **2013**, *111*, 1364–1372.

(24) Steiner, E.; Fowler, P. W.; Soncini, A.; Jenneskens, L. W. Current-Density Maps as Probes of Aromaticity: Global and Clar π Ring Currents in Totally Resonant Polycyclic Aromatic Hydrocarbons. *Faraday Discuss.* **2007**, *135*, 309–323.

(25) Sundholm, D.; Berger, R. J. F.; Fliegl, H. Analysis of the Magnetically Induced Current Density for Molecules Consisting of Annelated Aromatic and Antiaromatic Hydrocarbon Rings. *Phys. Chem. Chem. Phys.* **2016**, *18*, 15934–15942.

(26) Fliegl, H.; Valiev, R. R.; Pichierri, F.; Sundholm, D. Theoretical Studies as a Tool for Understanding the Aromatic Character of Porphyrinoid Compounds. *Chem. Modell.* **2018**, *14*, 1–42.

(27) Cherni, E.; Champagne, B.; Ayadi, S.; Liegeois, V. Magnetically-Induced Current Density Investigation in Carbohelicenes and Azahelicenes. *Phys. Chem. Chem. Phys.* **2019**, *21*, 14678–14691.

(28) Kupka, T.; Gajda, Ł.; Stobiński, L.; Kołodziej, Ł.; Mnich, A.; Buczek, A.; Broda, M. A. Local Aromaticity Mapping in the Vicinity of Planar and Nonplanar Molecules. *Magn. Reson. Chem.* **2019**, *57*, 359–372.

(29) Dressler, J. J.; Zhou, Z.; Marshall, J. L.; Kishi, R.; Takamuku, S.; Wei, Z.; Spisak, S. N.; Nakano, M.; Petrukhina, M. A.; Haley, M. M. Synthesis of the Unknown Indeno[1,2-*a*]fluorene Regioisomer: Crystallographic Characterization of Its Dianion. *Angew. Chem. Int. Ed.* **2017**, *56*, 15363–15367.

(30) Bheemireddy, S. R.; Ubaldo, P. C.; Finke, A. D.; Wang, L.; Plunkett, K. N. Contorted Aromatics via a Palladium-Catalyzed Cyclopentannulation Strategy. *J. Mater. Chem. C* **2016**, *4*, 3963–3969.

(31) Konishi, A.; Okada, Y.; Kishi, R.; Nakano, M.; Yasuda, M. Enhancement of Antiaromatic Character via Additional Benzoannulation into Dibenzo[*a,f*]pentalene: Syntheses and Properties of Benzo[*a*]naphtho[2,1-*f*]pentalene and Dinaphtho[2,1-*a,f*]pentalene. *J. Am. Chem. Soc.* **2019**, *141*, 560–571.

(32) Jin, Z.; Teo, Y. C.; Teat, S. J.; Xia, Y. Regioselective Synthesis of [3]Naphthylenes and Tuning of Their Antiaromaticity. *J. Am. Chem. Soc.* **2017**, *139*, 15933–15939.

(33) Skidin, D.; Eisenhut, F.; Richter, M.; Nikipar, S.; Krüger, J.; Ryndyk, D. A.; Berger, R.; Cuniberti, G.; Feng, X.; Moresco, F. On-Surface Synthesis of Nitrogen-Doped Nanographenes with 5–7 Membered Rings. *Chem. Commun.* **2019**, *55*, 4731–4734.

(34) Firmansyah, D.; Deperasińska, I.; Vakuliuk, O.; Banasiewicz, M.; Tasior, M.; Makarewicz, A.; Cyrański, M. K.; Kozankiewicz, B.; Gryko, D. T. Double Head-to-

Tail Direct Arylation as a Viable Strategy Towards the Synthesis of the Aza-Analog of Dihydrocyclopenta[hi]aceanthrylene - an Intriguing Antiaromatic Heterocycle. *Chem. Commun.* **2016**, *52*, 1262–1265.

(35) Cruz, C. M.; Castro-Fernández, S.; Maçôas, E.; Cuerva, J. M.; Campaña, A. G. Undecabenzo[7]superhelicene: A Helical Nanographene Ribbon as a Circularly Polarized Luminescence Emitter. *Angew. Chem. Int. Ed.* **2018**, *57*, 14782–14786.

(36) Márquez, I. R.; Fuentes, N.; Cruz, C. M.; Puente-Muñoz, V.; Sotorrios, L.; Marcos, M. L.; Choquesillo-Lazarte, D.; Biel, B.; Crovetto, L.; Gómez-Bengoa, E. et al. Versatile Synthesis and Enlargement of Functionalized Distorted Heptagon-Containing Nanographenes. *Chem. Sci.* **2017**, *8*, 1068–1074.

(37) Fukui, N.; Kim, T.; Kim, D.; Osuka, A. Porphyrin Arch-Tapes: Synthesis, Contorted Structures, and Full Conjugation. *J. Am. Chem. Soc.* **2017**, *139*, 9075–9088.

(38) Żyła, M.; Gońka, E.; Chmielewski, P. J.; Cybińska, J.; Stępień, M. Synthesis of a Peripherally Conjugated 5-6-7 Nanographene. *Chem. Sci.* **2016**, *7*, 286–294.

(39) Kawasumi, K.; Zhang, Q.; Segawa, Y.; Scott, L. T.; Itami, K. A Grossly Warped Nanographene and the Consequences of Multiple Odd-Membered-Ring Defects. *Nat. Chem.* **2013**, *5*, 739–744.

(40) Pun, S. H.; Chan, C. K.; Luo, J.; Liu, Z.; Miao, Q. A Dipleiadiene-Embedded Aromatic Saddle Consisting of 86 Carbon Atoms. *Angew. Chem. Int. Ed.* **2018**, *57*, 1581–1586.

(41) Mishra, S.; Krzeszewski, M.; Pignedoli, C. A.; Ruffieux, P.; Fasel, R.; Gryko, D. T. On-Surface Synthesis of a Nitrogen-Embedded Buckybowl with Inverse Stone–Thrower–Wales Topology. *Nat. Commun.* **2018**, *9*, 1714.

(42) Sundholm, D.; Fliegl, H.; Berger, R. J. Calculations of Magnetically Induced Current Densities: Theory and Applications. *WIREs Comput. Mol. Sci.* **2016**, *6*, 639–678.
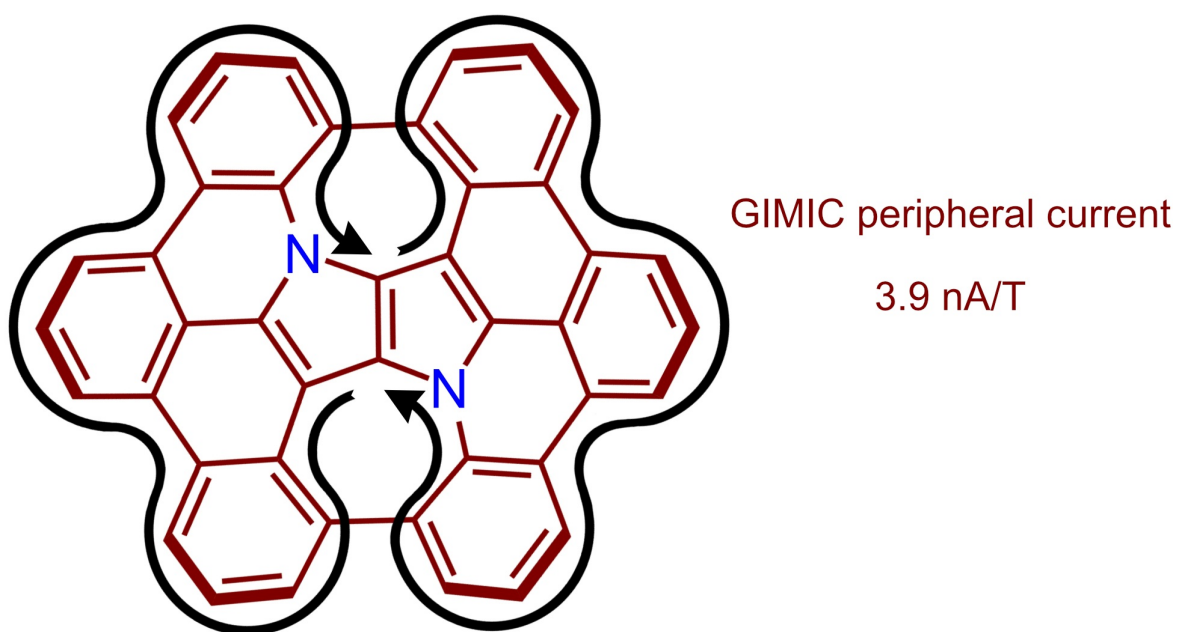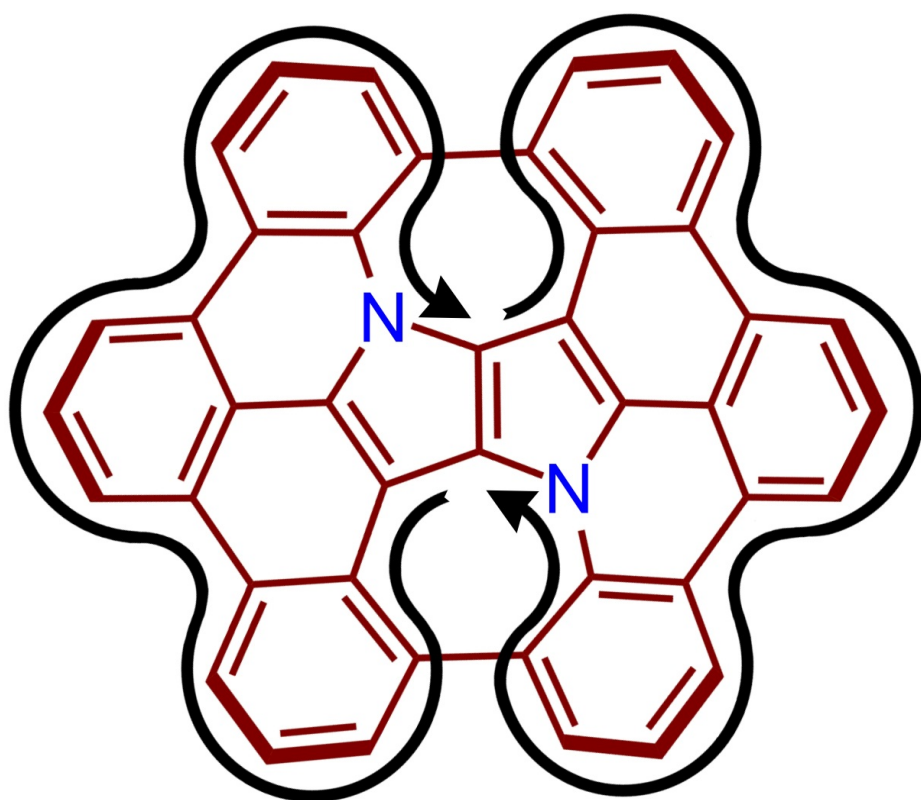
(43) Gershoni-Poranne, R.; Stanger, A. Magnetic Criteria of Aromaticity. *Chem. Soc. Rev.* **2015**, *44*, 6597–6615.

(44) Geuenich, D.; Hess, K.; Kohler, F.; Herges, R. Anisotropy of the Induced Current Density (ACID), a General Method to Quantify and Visualize Electronic Delocalization. *Chem. Rev.* **2005**, *105*, 3758–3772.

(45) Oki, K.; Takase, M.; Mori, S.; Shiotari, A.; Sugimoto, Y.; Ohara, K.; Okujima, T.; Uno, H. Synthesis, Structures, and Properties of Core-Expanded Azacoronene Analogue: A Twisted π-System with Two N-Doped Heptagons. *J. Am. Chem. Soc.* **2018**, *140*, 10430–10434.

(46) Jusélius, J.; Sundholm, D.; Gauss, J. Calculation of Current Densities Using Gauge-Including Atomic Orbitals. *J. Chem. Phys.* **2004**, *121*, 3952–3963.

(47) Fliegl, H.; Taubert, S.; Lehtonen, O.; Sundholm, D. The Gauge Including Magnetically Induced Current Method. *Phys. Chem. Chem. Phys.* **2011**, *13*, 20500–20518.

(48) GIMIC, Version 2.0, a Current Density Program. Can be freely downloaded from https://github.com/qmcurrents/gimic.

(49) Ahlrichs, R.; Bär, M.; Häser, M.; Horn, H.; Kölmel, C. Electronic Structure Calculations on Workstation Computers: The Program System TURBOMOLE. *Chem. Phys. Lett.* **1989**, *162*, 165–169, current version: See http://www.turbomole.com.

(50) Furche, F.; Ahlrichs, R.; Hättig, C.; Klopper, W.; Sierka, M.; Weigend, F. Turbomole. *WIREs Comput. Mol. Sci.* **2014**, *4*, 91–100.

(51) Becke, A. D. Density-Functional Exchange-Energy Approximation with Correct Asymptotic Behavior. *Phys. Rev. A* **1988**, *38*, 3098–3100.

(52) Becke, A. D. Density-Functional Thermochemistry. III. The Role of Exact Exchange. *J. Chem. Phys.* **1993**, *98*, 5648–5652.

(53) Lee, C.; Yang, W.; Parr, R. G. Development of the Colle-Salvetti Correlation-Energy Formula into a Functional of the Electron Density. *Phys. Rev. B* **1988**, *37*, 785–789.

(54) Weigend, F.; Ahlrichs, R. Balanced Basis Sets of Split Valence, Triple Zeta Valence and Quadruple Zeta Valence Quality for H to Rn: Design and Assessment of Accuracy. *Phys. Chem. Chem. Phys.* **2005**, *7*, 3297–3305.

(55) Häser, M.; Ahlrichs, R.; Baron, H. P.; Weis, P.; Horn, H. Direct Computation of 2nd-order SCF Properties of Large Molecules on Workstation Computers with an Application to Large Carbon Clusters. *Theoret. Chim. Acta* **1992**, *83*, 455–470.

(56) Kollwitz, M.; Häser, M.; Gauss, J. Non-Abelian Point Group Symmetry in Direct Second-Order Many-Body Perturbation Theory Calculations of NMR Chemical Shifts. *J. Chem. Phys.* **1998**, *108*, 8295–8301.

(57) Reiter, K.; Mack, F.; Weigend, F. Calculation of Magnetic Shielding Constants with Meta-GGA Functionals Employing the Multipole-Accelerated Resolution of the Identity: Implementation and Assessment of Accuracy and Efficiency. *J. Chem. Theory Comput.* **2018**, *14*, 191–197.

(58) Grimme, S.; Antony, J.; Ehrlich, S.; Krieg, H. A Consistent and Accurate Ab Initio Parametrization of Density Functional Dispersion Correction (DFT-D) for the 94 Elements H-Pu. *J. Chem. Phys.* **2010**, *132*, 154104.

(59) Stanger, A. Reexamination of $NICS_{\pi,zz}$: Height Dependence, Off-Center Values, and Integration. *J. Phys. Chem. A* **2019**, *123*, 3922–3927.

(60) Stanger, A. The Different Aromatic Characters of Some Localized Benzene Derivatives. *J. Phys. Chem. A* **2008**, *112*, 12849–12854.

(61) Messersmith, R. E.; Tovar, J. D. Borepin Rings as "Sigma-Free" Reporters of Aromaticity within Polycyclic Aromatic Scaffolds. *J. Phys. Chem. A* **2019**, *123*, 881–888.

(62) Jousselin-Oba, T.; Deal, P. E.; Fix, A. G.; Frederickson, C. K.; Vonnegut, C. L.; Yassar, A.; Zakharov, L. N.; Frigoli, M.; Haley, M. M. Synthesis and Properties of Benzo-Fused Indeno[2,1-c]fluorenes. *Chem. Asian J.* **2019**, *14*, 1737–1744.

(63) Gershoni-Poranne, R.; Stanger, A. The NICS-XY-Scan: Identification of Local and Global Ring Currents in Multi-Ring Systems. *Chem. Eur. J.* **2014**, *20*, 5673–5688.

(64) Stanger, A.; Monaco, G.; Zanasi, R. NICS-XY-Scan Predictions of Local, Semi-Global, and Global Ring Currents in Annulated Pentalene and s-Indacene Cores Compared to First-Principles Current Density Maps. *ChemPhysChem*, in press, DOI: 10.1002/cphc.201900952.

(65) Stanger, A. Obtaining Relative Induced Ring Currents Quantitatively from NICS. *J. Org. Chem.* **2010**, *75*, 2281–2288.

(66) Rahalkar, A.; Stanger, A., "Aroma" package;
https://chemistry.technion.ac.il/members/amnonstanger/.

(67) Stanger, A. Nucleus-Independent Chemical Shifts (NICS): Distance Dependence and Revised Criteria for Aromaticity and Antiaromaticity. *J. Org. Chem.* **2006**, *71*, 883–893.

(68) Krzeszewski, M.; Kodama, T.; Espinoza, E. M.; Vullev, V. I.; Kubo, T.; Gryko, D. T. Nonplanar Butterfly-Shaped π-Expanded Pyrrolopyrroles. *Chem. Eur. J.* **2016**, *22*, 16478–16488.

(69) Tokimaru, Y.; Ito, S.; Nozaki, K. A Hybrid of Corannulene and Azacorannulene: Synthesis of a Highly Curved Nitrogen-Containing Buckybowl. *Angew. Chem. Int. Ed.* **2018**, *57*, 9818–9822.

(70) Clar, E. *The Aromatic Sextet*; Wiley: New York, 1972.

(71) Balaban, A.; von Ragué Schleyer, P.; Rzepa, H. S. Crocker, Not Armit and Robinson, Begat the Six Aromatic Electrons. *Chem. Rev.* **2005**, *105*, 3436–3447.

(72) Soncini, A.; Steiner, E.; Fowler, P. W.; Havenith, R. W. A.; Jenneskens, L. W. Perimeter Effects on Ring Currents in Polycyclic Aromatic Hydrocarbons: Circumcoronene and Two Hexabenzocoronenes. *Chem. Eur. J.* **2003**, *9*, 2974–2981.

1
2
3
4
5
6
7
8
9
10
11
12
13
14
15
16
17
18
19
20
21
22
23
24
25
26
27
28
29
30
31
32
33
34
35
36
37
38
39
40
41
42
43
44
45
46
47
48
49
50
51
52
53
54
55
56
57
58
59
60

GIMIC peripheral current

3.9 nA/T

1
2
3
4
5
6
7
8
9
10
11
12
13
14
15
16
17
18
19
20
21
22
23
24
25
26
27
28
29
30
31
32
33
34
35
36
37
38
39
40
41
42
43
44
45
46
47
48
49
50
51
52
53
54
55
56
57
58
59
60

GIMIC peripheral current

3.9 nA/T